Dyes and Pigments 203 (2022) 110310

Contents lists available at ScienceDirect

Dyes and Pigments

journal homepage: www.elsevier.com/locate/dyepig

Enhancing the temporal stability of DSSCs with novel vinylpyrimidine anchoring and accepting group

Isolda Duerto [a], Santiago Sarasa [a], Daniel Barrios [b], Jesús Orduna [a], Belén Villacampa [b], María-Jesús Blesa [a,*]

[a] Departamento de Química Orgánica, INMA, Universidad de Zaragoza-CSIC, 50009, Zaragoza, Spain
[b] Departamento de Física de la Materia Condensada, INMA, Universidad de Zaragoza-CSIC, 50009, Zaragoza, Spain

ARTICLE INFO

Keywords:
Vinylpyrimidine
Metal-free sensitizer
Anchoring group
Aggregation
Temporal stability

ABSTRACT

Three compounds based on aniline, thiophene and vinylpyrimidine as anchoring group have been prepared and studied as light harvesting units for dye-sensitized solar cells (DSSCs). They comprise thiophenyl π-spacer systems with one or two thiophenes (**AT-Pyri, ATT-Pyri)** and aniline as donor which is functionalized, in one case, with an hydroxyl group (**HO-AT-Pyri**). The bithiophene based dye (**ATT-Pyri**) shows higher extinction coefficients and smaller transition energy, as well as broader absorption spectrum. Thus, despite lower dye uptake, devices based on one thiophene and with the hydroxyl group (**HO-AT-Pyri**) have slightly higher power conversion efficiencies (η) as compared with the analogous dye without this group (**AT-Pyri**). However, the best performing device is based on the dye with bithiophene bridge (**ATT-Pyri)** when a co-adsorbent is added to avoid the aggregation of the dye. The photovoltaic parameters of cells based on these vinylpyrimidine dyes are enhanced over 1000 h, especially for **ATT-Pyri** devices, which reach a η = 6,4%.

1. Introduction

Dyes sensitized solar cells (DSSCs), firstly described by Gräztel [1], are already established as a portable and flexible alternative to conventional solar cells [2]. They are formed by a photoanode and a counter electrode assembled with an electrolyte between them. The dye that sensitizes the photoanode is considered the key element for this kind of cells. In general, the chromophores chosen for this application are Donor-π-Acceptor (D-π-A) systems, which have a versatile structure that allows properties tailoring, providing the opportunity to find structure-properties relationships based on photophysical and electrochemical characteristics.

With respect to the donor part, *N, N*-dialkylanilines have been used in solar cells, due to their simple structure and their electrondonor capacity [3]. Different studies have shown that dyes with this donor [4] have good properties in terms of light absorption, showing the charge transfer band bathochromically shifted with respect to the widely used triphenylamine derivatives (TPA) [5,6].

Thiophene heteroaromatic rings are used as π-conjugated bridge because they give stability to the D-π-A system in addition to expanding the conjugation path. As a consequence, a red shift of the absorption maximum as well as an enhancement of the molar extinction coefficient is observed with respect to the double bond bridge. Longer thiophene chains as bithiophene is reported [7] to improve the photovoltaic properties when *N, N*-dialkylanilines are used as donors. However, it is reported that it is no convenient to use quaterthiophene as π-spacer [8] because those dyes would be more likely to aggregate.

As a rule, conventional sensitizers have been designed using cyanoacetic group with anchoring and accepting functions. The cyano group has strong electron withdrawing properties that have been previously studied [9] while the acidic group is the one that binds the dye to TiO_2 [10]. In addition to this classic system, a few [11] new types of sensitizers have been designed with other acceptors such as rhodanine [12], pyridine [13], 3-hydroxylpyridium [14], salicylic acid [15] and hydroxyquinoline [16], etc. Dyes with pyridyl groups have been reported to be linked to TiO_2 predominantly through a coordinated bond between the pyridyl group and the Lewis acid sites (Ti^{n+}) on the surface of TiO_2. These dyes can inject electrons into the TiO_2 conduction band through this bonding [17]. In this context, pyrimidine (1,3-diazine) also has a π-deficient aromatic character and can act as electron-withdrawing

* Corresponding author.
E-mail addresses: isolda@unizar.es (I. Duerto), santi.s.sanjo@gmail.com (S. Sarasa), danielb@unizar.es (D. Barrios), jorduna@unizar.es (J. Orduna), bvillaca@unizar.es (B. Villacampa), mjblesa@unizar.es (M.-J. Blesa).

https://doi.org/10.1016/j.dyepig.2022.110310
Received 8 February 2022; Received in revised form 15 March 2022; Accepted 3 April 2022
Available online 14 April 2022

group in D-π-A chromophores. This novel acceptor and anchoring group allows chelation, protonation and hydrogen-bond formation with the participation of the nitrogen atoms of the pyrimidine [18]. Hence, dyes with this group could be also used as sensors or to form supramolecular assemblies. As far as we know there are no studies about only vinylpyrimidine acting as acceptor groups in dyes for DSSC. Pyrimidine appears as a building block in several studies [19–23] but always with a carboxylic acid in the molecule. Wu et al. [16] designed and synthesized a dye with pyrimidine-2-carboxylic acid as an electron-accepting and anchoring groups. Both the carboxylic group and the two adjacent nitrogen atoms are presumed to form two coordination bonds with the titanium atoms of TiO_2. Ooyama et al. developed more complex D-π-A systems with two anchoring groups: an analogous nitrogen heterocycle, the pyrazyl, which acts as electro withdrawing anchoring group and also a carboxylic acid σ-linked to these D-π-A systems. However, in this case their efficiency reached only 1.58% [20].

In this work, the preparation of dyes with aniline (**A**) as donor and pyrimidine (**Pyri**) as novel vinylpyrimidine-acceptor and anchoring group is proposed. Thiophene (**T**) and bithiophene (**TT**) are used as π-spacers to compare the effect of the extension of the conjugation on the charge transfer. Furthermore, the structure of the dye **AT-Pyri** is modified with the introduction of a hydroxyl group (**OH**) with the aim to study the effect of this ancillary anchoring group on both the dye loading and the electron transfer properties (Chart 1). Besides, the effect of these factors on the photovoltaic performance of the devices has been analyzed paying attention to the long-term stability of the response. Furthermore, the structure-properties relationship of these novel dyes has been analyzed.

2. Results and discussion

2.1. Synthesis

Synthesis of dyes **AT-Pyri, ATT-Pyri** and **HO-AT-Pyri** is depicted in Scheme 1.

The aldehydes 5-(4-dimethylaminophenyl)thiophenyl-2-carbaldehyde (**AT-CHO**) [24] and 5' -(4-dimethylaminophenyl)-[2,2']-bithiophenyl-5-carbaldehyde (**ATT-CHO**) were prepared following the procedure described in the literature [25] and the starting aldehyde **SIL-A-T-CHO** was synthesized by Gonzalez et al. [26].

The dyes **AT-Pyri, ATT-Pyri** and **HO-AT-Pyri** were obtained by condensation between 4-methylpyrimidine and the corresponding aldehydes, **AT-CHO, ATT-CHO** and **SIL-A-T-CHO,** respectively. It was used boiling aqueous 5 M NaOH with a phase-transfer catalyst, Aliquat 336. This protocol gives a variety of vinylpyrimidines [18,27].

This experimental method offers easy access, in yields between 48 and 95%, to give different vinylpyrimidines derivatives with aniline as electron-donating group and thiophene/s as π-spacer/s. The characterization of dyes is reported in Supporting Information (Figures S.13 and S.21).

2.2. Optical properties

The UV–vis absorption measurements were carried out in CH_2Cl_2 solutions (10^{-5} M <) and on sensitized TiO_2 films. Fig. 1 shows the UV–vis spectra of the dyes **AT-Pyri, ATT-Pyri** and **HO-AT-Pyri.** The spectra of thiophene derivatives, **AT-Pyri** and **HO-AT-Pyri**, show almost identical bands in the visible region (350–500 nm) whereas the absorption band of bithiophene derivative **ATT-Pyri**, something broader and red shifted, extends up to 550 nm. In all cases, the bands are attributed to the intramolecular charge transfer between the electron-withdrawing and electron-donating parts of these dyes. Considering

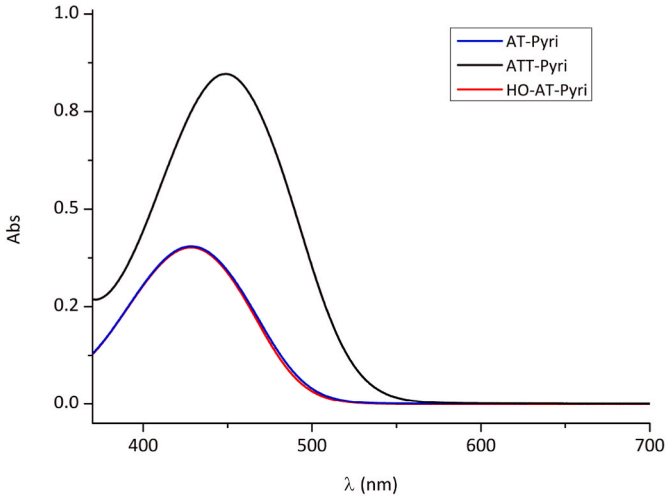

Fig. 1. UV–vis spectra of the dyes **AT-Pyri, ATT-Pyri** and **HO-AT-Pyri** in solution (10^{-5} M CH_2Cl_2).

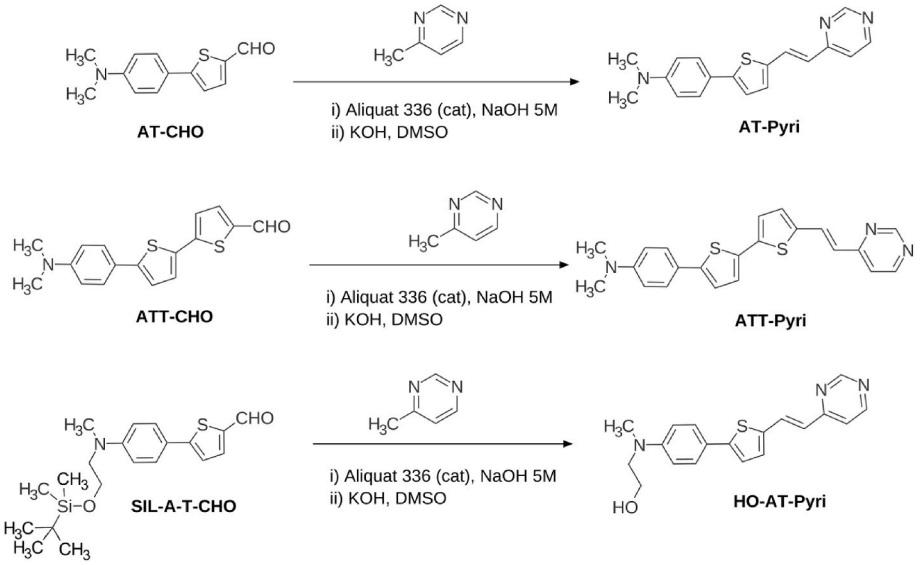

Scheme 1. Synthesis of dyes **AT-Pyri, ATT-Pyri** and **HO-AT-Pyri.**

the broader absorption band of **ATT-Pyri**, as compared with the shorter dye, quite higher photocurrent density (J_{sc}) values can be expected [28].

Fig. 2 a) shows the UV–vis spectra of the dye **HO-AT-Pyri** in solution and adsorbed on a TiO_2 film (after 5 h of immersion in dye solution). The spectrum of the film shows a hypsochromic shift of the ICT band with respect to that measured in solution, which can be attributed to the adsorption of the dye on the TiO_2 [29] or to aggregation effects. Trying to obtain further insight about the origin of the shift, several studies based on UV–vis measurements and ATR-FTIR results have been carried out. As concerns optical studies in solution, a series of protonation runs was carried out by the addition of an excess of trifluoroacetic acid (TFA) in order to simulate the conditions of the linkage of the dye to the TiO_2 film. In addition, the absorption of films with chenodeoxycholic acid (CDCA), which was used as co-adsorbent to prevent dye aggregation, was also measured (Fig. 2).

The spectra of **HO-AT-Pyri** (Fig. 2 a) show the difference between the absorption of the dye in the CH_2Cl_2 solution and the one with an excess of acid. The hypsochromically shifted band associated with the acidic solution is similar to the band of the TiO_2 film which points to low aggregation in films prepared with **HO-AT-Pyri** dye. It can be concluded that, in this case, the main contribution to the shift is the linkage of the dye to the TiO_2. However, the spectra of **ATT-Pyri** (Fig. 2 b) suggest that the two contributions are important, since the shift observed when an excess of acid is present is clearly smaller than the obtained in films. In addition, the difference between spectra with and without CDCA supports the relevance of aggregation which explains the total shift.

The optical properties of the three dyes are summarized in Table 1. The molar extinction coefficient of the **ATT-Pyri** (ε) is double that of **AT-Pyri** and **HO-AT-Pyri,** so good light-absorption ability is expected for this new sensitizer for DSSCs. The spectra used to calculate these molar extinction coefficients are reported in Figures S.1-S.3 in Electronic Supporting Information. Moreover, the study of photoanode immersion time in dye solutions is also gathered in Electronic Supporting Information (Figures S.4-S.6.).

2.3. Electrochemical properties

The redox properties of the dyes **AT-Pyri, ATT-Pyri** and **HO-AT-Pyri** were explored by Differential Pulse Voltammetry (DPV). 0.1 M tetrabutylammonium hexafluorophosphate was used as supporting electrolyte, a glassy carbon as working electrode, a Pt thread as counter electrode and the reference electrode was made of Ag/AgCl. The dye concentrations of dye solutions in CH_2Cl_2 was $5 \cdot 10^{-4}$ M. The oxidation potential of both ground and excited states of **AT-Pyri, ATT-Pyri** and **HO-AT-Pyri** dyes are depicted in Table 1 showing that the redox process of **ATT-Pyri** dye is easier than those of **AT-Pyri** and **HO-AT-Pyri**. The potential value of **ATT-Pyri** is 0.07 V lower than the one of **AT-Pyri** dye because the bithiophene is stronger donor that thiophene and therefore it causes a higher HOMO energy. This explanation has been corroborated with the theoretical calculation shown in section 2.4. The corresponding voltammograms and the diagram of energy are reported in the Electronic Supporting Information (Figures S.7-S.10). It must be considered that the oxidation potential of the excited state of the dye, E_{ox}* value, must be more negative than the TiO_2 conduction band (– 0.5 V vs NHE) [30] and the oxidation potential of the ground state of the dye, E_{ox} value, must be more positive than the redox potential of the I_3^-/I^- electrolyte (+0.4 V) [31]. In accordance with these requirements, it can be seen that E_{ox}* values (Table 1) favor the electron injection from the excited dye onto the TiO_2 and E_{ox} values ensure that the dyes are effectively regenerated after being oxidized.

Table 1
Optical parameters, transition energy $E_{0\text{-}0}$ and potential values E_{ox} *and* E_{ox}*.

Dye	λ_{abs} [a] (nm)	λ_{cut} (nm)	ε [a] (10^4 $M^{-1}\cdot cm^{-1}$)	$E_{0\text{-}0}$ [b] (eV)	E_{ox} [c] (V)	E^*_{ox} [d] (V)
AT-Pyri	428	528	1.98 ± 0.02	2.35	0.88	−1.47
ATT-Pyri	449	550	3.89 ± 0.01	2.25	0.81	−1.44
HO-AT-Pyri	428	528	1.86 ± 0.01	2.35	0.88	−1.47

[a] In CH_2Cl_2 solution.
[b] $E_{0\text{-}0}$ was estimated from λ_{cut} value in the absorption spectrum, $E_{0\text{-}0} = 1239.84/\lambda_{cut}$.
[c] The oxidation potentials were converted to normal hydrogen electrode (NHE) by addition of 0.199 V.
[d] The estimated oxidation potential of excited state of the dye (E^*_{ox}) was calculated from $E^*_{ox} = E_{ox} - E_{0\text{-}0}$.

2.4. Theoretical calculations

The electronic structure of the new synthesized dyes has been studied using DFT (Density Functional Theory) calculations. The most relevant calculated parameters are gathered in Table 2 and it can be seen that they compare fairly well to the experimental parameters shown in Table 1.

The lowest energy electronic transition is associated in every case to an intense absorption band (corresponding to high oscillator strength) that according to the calculations is mainly contributed from a one electron promotion from the HOMO to the LUMO (see Fig. 3). The location of the HOMO on the donor group and the LUMO on the acceptor pyrimidine gives this transition an Intramolecular Charge Transfer (ICT) character while the large HOMO-LUMO overlap on the bithiophene spacer gives rise to large oscillator strengths. The calculated values account for the higher extinction coefficient (and therefore higher light harvesting efficiency) and the bathochromic shift of **ATT Pyri** compared to the other two dyes.

The contour plot of the spin density calculated for oxidized radical-

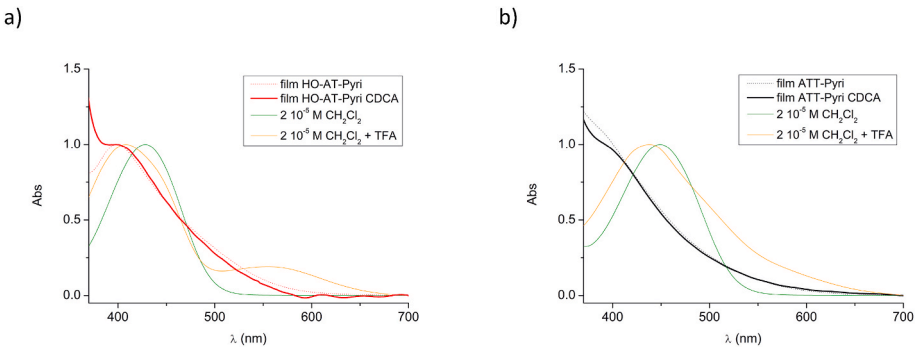

Fig. 2. a) UV-vis spectrum in CH_2Cl_2 solution of **HO-AT-Pyri** without (green) and with (orange) TFA vs UV-vis spectrum in film of **HO-AT-Pyri** dye after 5h of immersion without (red —) and with CDCA (red _). b) UV-vis spectrum in CH_2Cl_2 solution of **ATT-Pyri** without (green) and with (orange) TFA vs UV-vis spectrum in film of **ATT-Pyri** dye after 5h of immersion without (black —) and with CDCA (black _).

Table 2
Calculated[a] parameters for compounds **AT-Pyri, ATT-Pyri** and **HO-AT-Pyri**.

Dye	λ_{abs}[a] (nm)	*f*	E_{HOMO} (eV)	E_{LUMO} (eV)	$E_{0\text{-}0}$ (eV)	E_{ox}[b] (V)	E^*_{ox}[b,c] (V)
AT Pyri	416	1.47	−6.38	−1.60	2.52	0.88	−1.63
ATT Pyri	443	1.77	−6.13	−1.32	2.34	0.86	−1.49
HO-AT-Pyri	410	1.50	−6.47	−1.61	2.53	1.03	−1.50

[a] Calculated using the *M06–2x/6-311+G(2d,p)* model chemistry and the *CPCM* solvation model in CH_2Cl_2. Equilibrium *CPCM* values.
[b] Referenced to Normal Hydrogen Electrode (NHE).
[c] The oxidation potential of the excited state of the dye was calculated from $E^*_{ox} = E_{ox} - E_{0\text{-}0}$. *f*: oscillator strength.

cations formed by the extraction of an electron dyes provides a representation of the electronic hole generated during the operation of the photovoltaic cell (Fig. 4).

It can be seen that this hole is mainly located over the donor and the spacer but the spin density on pyrimidine anchor group is scarce. This may have a beneficial effect by hindering the undesirable back electron transfer from the TiO_2 electrode to the dye.

The negligible contribution of the pyrimidine ring to the spin density in **ATT-Pyri** along with the higher light harvesting efficiency of this dye suggest it is a better candidate for efficient DSSCs.

2.5. FTIR spectra

As a rule, Fourier transform infrared spectroscopy (FTIR) in transmission is the material characterization tool dedicated to the structural examination of adsorption modes at the anchor/substrate interface. Unfortunately, conventional transmission-based FTIR has yielded poor signal-to-noise ratios. Hence, attenuated total reflection (ATR-FTIR) is used instead. The capabilities of ATR-FTIR allow the wave to propagate along the region near the dye/TiO_2 interface, which enhances the anchor-specific signal [32].

Fig. 5 and Figure S.11 exhibit the ATR-FTIR spectra of the dye powder and adsorbed on TiO_2 to study the adsorption of the dyes **AT-Pyri, ATT-Pyri** and **HO-AT-Pyri** dyes on TiO_2. The spectra of the powder of these dyes show the characteristic stretching vibration bands for C═N which are observed at around 1575 and 1429 cm^{-1} and the C═C vibration at 1600 cm^{-1}. However, in the spectra of dyes adsorbed on TiO_2 a shift of the characteristic stretching bands for C═N was observed. The vibrations at 1600 and 1450 cm^{-1} can be attributed to the nitrogen of the pyrimidine ring coordinated to the Lewis acid sites of the TiO_2 surface (Ti^{n+} cations) as it was reported in the literature with the analogous nitrogen atom of pyridine [33–36]. The relevant increase of the 1600 cm^{-1} peak in the spectrum of TiO_2 film is due to a double contribution, the characteristic vibration of the bond C═C and the vibration attributed to the coordination bond formed between the Lewis region of the TiO_2 surface and the nitrogen atom of the pyrimidine ring of the photosensitizer. This result indicates that the pyrimidine ring may be an adequate electron-withdrawing anchoring group in these solar cells.

Moreover, the hydroxyl group of the dye **HO-AT-Pyri** allows the formation of hydrogen-bonds with the TiO_2. For the powder spectrum of **HO-AT-Pyri** the vibration of the C–O(H) bond was observed at 1192 cm^{-1}. The FTIR spectrum of powder sample shows the hyperfine structure. However, in the spectra of dyes adsorbed on TiO_2 film, the stretching vibrations have not hyperfine structure. Thus, these observations indicate that the dye **HO-AT-Pyri** is adsorbed on the TiO_2 surface through the formation of a linkage between the hydroxyl group of the **HO-AT-Pyri** dye and the TiO_2 surface of the photoanode [37].

2.6. Dye-sensitized solar cells

The previous sections suggest that compounds **AT-Pyri, ATT-Pyri** and **HO-AT-Pyri,** based on aniline-thiophene and pyrimidine can work as sensitizers and the pyrimidine ring may be a candidate as an anchoring group. The DSSCs have been built under the conditions chosen following our previous studies [38]. The electrolyte was the classical I_3^-/I^- system prepared in anhydrous acetonitrile (I_2 (0.050 M), LiI (0.10 M), 1-butyl-3-methylimidazolium iodide (0.53 M), and *tert*-butylpyridine (0.52 M)). The photoanode was sensitized by immersion in 0.1 mM

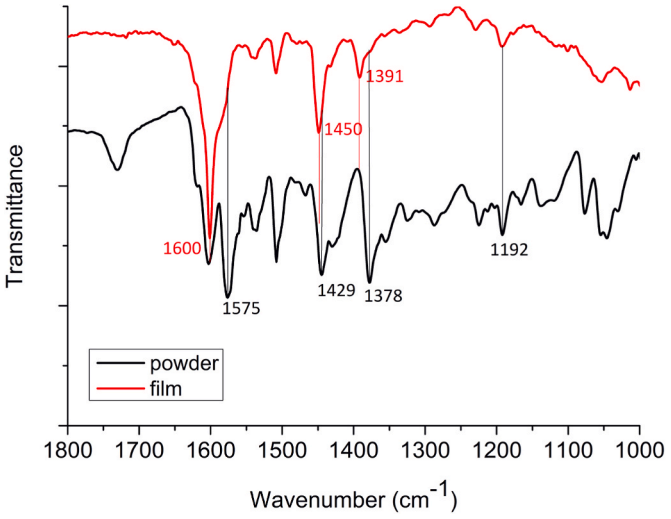

Fig. 5. ATR-FTIR spectra of the dyes **HO-AT-Pyri** a) adsorbed on TiO_2 (red line) and b) powder (black line).

Fig. 3. 0.04 Contour plots for the HOMO (left) and LUMO (right) of dye **ATT-Pyri**.

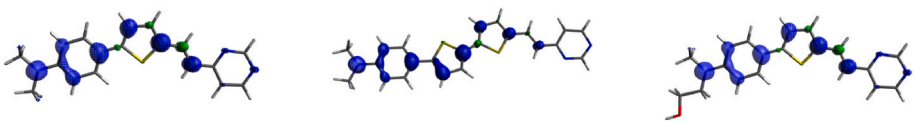

Fig. 4. 0.004 Contour plots of the spin density calculated for radical cations derived from **AT-Pyri** (left), **ATT-Pyri** (centre) and **HO-AT-Pyri** (right).

CH_2Cl_2 dye solutions (**HO-AT-Pyri, AT-Pyri** and **ATT-Pyri**) for 5 h.

The photovoltaic properties of these DSSCs (Figs. 6 and 7 and Tables 3 and 4) as well as the long-term stability of the characteristic parameters were evaluated (Fig. 8 and Table 5). Three analogous devices were prepared with each dye; and the average value of the parameters is included in the Electronic Supporting Information (Table S.1 and **S.2**).

Fig. 6 depicts that the short circuit photocurrent (J_{sc}) of the devices prepared with the dyes with one thiophene is higher when the oxygenate chain is linked to the aniline (**HO-AT-Pyri**). This is probably due to the fact that the hydroxyl group contributes to improve the current. The photovoltage (V_{oc}), is also higher for these cells as compared to those of **AT-Pyri**, suggesting that the chain *-CH_2CH_2OH* acts as a more effective blocking unit between the TiO_2 surface and the electrolyte than the methyl group in the case of the **AT-Pyri** device.

Moreover, cells with the co-adsorbent CDCA (0.3 mM) were prepared to improve the open-circuit photovoltage and also to study the effect of the co-adsorbent CDCA in aggregation and, consequently, in the performance of the corresponding devices. These results are shown in Fig. 7.

DSSCs prepared with **ATT-Pyri** has twice the dye loading of **AT-Pyri** in the case of cells without co-adsorbent, and four times in devices prepared with CDCA. There are some studies in the literature that report that the adsorption amount of dye with the longer π-spacers is higher than that of the shorter ones [8,39,40]. However, this increase is not directly reflected on the performance of this kind of cells because the larger dyes are more prone to aggregate than the shorter ones.

Fig. 7. (left) shows that the addition of the co-adsorbent CDCA improves considerably the photovoltage in every cell because CDCA makes difficult the electronic recombination between the TiO_2 and the electrolyte and the back-electron transfer (*BET*). However, the J_{sc} is only clearly increased in the case of **ATT-Pyri**, 47% over the initial value. Table 4 shows that the device prepared with **ATT-Pyri** and the co-adsorbent presents the highest efficiency of this series, 5.70%. The noticeable improvement 74% is explained by the antiaggregation effect of CDCA additive. The decrease of the photocurrent and, consequently, of the overall efficiency in **HO-AT-Pyri** devices is due to the significant decrease on dye loading when the co-adsorbent is present.

The incident photon to converted electron efficiency (IPCE) spectra (Fig. 7-right) depicts an intense and broad curve in the visible region up to 750 nm, especially for devices prepared with **ATT-Pyri** and CDCA. It is known that intense and broad IPCE spectra guarantee high photocurrent and consequently, a good efficiency. Hence, we can conclude that the co-adsorbent is efficiently suppressing aggregation, and therefore improving the performance of these cells.

Moreover, it is observed that the amount of dye on the photoanodes prepared with **HO-AT-Pyri** is higher than on photoanodes with **AT-Pyri.**

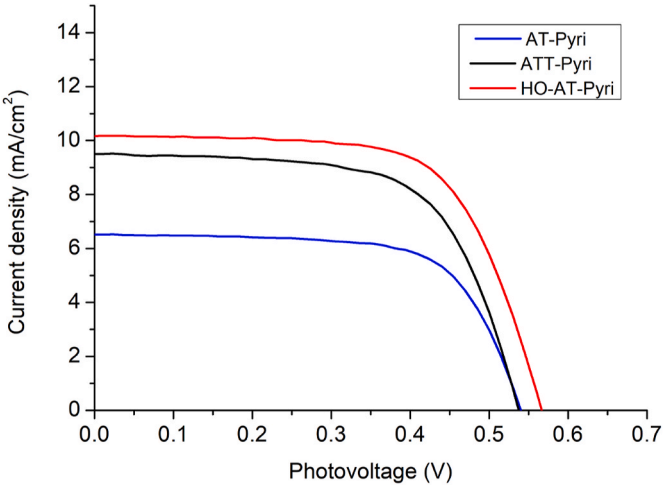

Fig. 6. Photocurrent-voltage plots of DSSCs without co-adsorbent CDCA.

It confirms that the adsorption of this difunctionalized dye is better than that of **AT-Pyri** dye.

The photovoltaic parameters have been also followed up to 1000 h in order to study the stability of the device performance. The results are gathered in Fig. 8 and Table 5.

Fig. 8 plots the stability studies of the cells where the evolution of higher efficiency up to 1000 h has been analyzed. It is worth mentioning that the devices prepared with co-adsorbent improve over the time when using the bithiophene dye (**ATT-Pyri**) (Table 5). This effect is particularly noticeable, showing an increase of 33% (up to $\eta = 4.36\%$) after 1000 h with respect to the values measured after 24 h. This result was already observed in our group with double dyes prepared with 3-methyl-1,1-cyclohexane as scaffold [7]. As a rule, it can be said that the efficiency values of all devices prepared with these novel dyes are increased for a period of several weeks.

Electrochemical Impedance Spectroscopy (*EIS*) measurements were carried out to get some information about the charge transfer and transport processes in cells prepared with dyes **AT-Pyri, ATT-Pyri** and **HO-AT-Pyri.** The devices were studied under dark conditions (0.8 V) 24 h after assembly and the Nyquist and Bode plots of cells were analyzed.

The intermediate frequency semicircle radio (the larger one in Figure S.12 –left) in the Nyquist plots is attributed to the charge recombination resistance (R_{rec}) at the TiO_2/dye/electrolyte interface. In this series, the resistance decreased following the sequence **HO-AT-Pyri > AT-Pyri > ATT-Pyri**. The R_{rec} values are 13.1, 11.2, 9.4 Ω, respectively (Figure S.12 -left), which is in accordance with the tendency of V_{oc} values (Table 4).

The Bode plots exhibit two peak features; the first one, at higher frequencies, is attributed to the charge transfer at the Pt/electrolyte interface, while the second one, at the intermediate frequency range lower is associated with charge transfer at the TiO_2/dye/electrolyte interface. The reciprocal of the frequency maximum of this latter peak (f) is associated with the electron lifetime in the conduction band of TiO_2, $\tau = 1/(2\pi f)$. In this series, the main difference is observed in the intermediate frequency range (Figure S.12-right). As can be seen in the figure, the peak of the **HO-AT-Pyri** cell shifts to a significant lower frequency (compared to the **AT-Pyri, ATT-Pyri** cells) the estimated τ values were 1.9, 1.3 and 0.8 ms for devices prepared with **HO-AT-Pyri, AT-Pyri** and **ATT-Pyri,** respectively. *EIS* results suggest that the *-CH_2CH_2OH* chains of **HO-AT-Pyri** act as effective blocking units between the TiO_2 surface and the electrolyte, preventing hydrophilic I_3^- ions approaching the TiO_2 surface and thereby leading to suppressed electron back reaction and lengthened electron lifetimes [41]. These facts also explain the higher V_{oc} of the **HO-AT-Pyri** cell as compared to **AT-Pyri** and **ATT-Pyri** cells (Tables 3 and 4).

3. Conclusions

Three novel dyes, which comprise aniline, thiophene/s and vinylpyrimidine as anchoring and accepting group, have demonstrated their capabilities as sensitizers in solar cells.

Photovoltaic properties are improved when the longer **ATT-Pyri** dye is used, compared to the one with a single thiophene, **AT-Pyri**. Due to the aggregation tendency of the dye with bithiophene, the improvement is much more evident when the co-adsorbent CDCA is incorporated to the photoanode.

The dye **HO-AT-Pyri** adsorbed on the TiO_2 surface through the formation of a linkage between the hydroxyl group and the TiO_2 contributes to a higher adsorption of dye and also enhance the photovoltaic properties of the cells because acts as an effective unit which contributes to improve both the photocurrent and photovoltage. However, the increase of the amount of dye on **ATT-Pyri,** having twice the dye loading of **AT-Pyri** in the case of cells without CDCA, and almost four times with CDCA, is not reflected on cell performance because of the aggregation tendency of the long **ATT-Pyri** dye.

The devices maintain or even increase the efficiency for more than

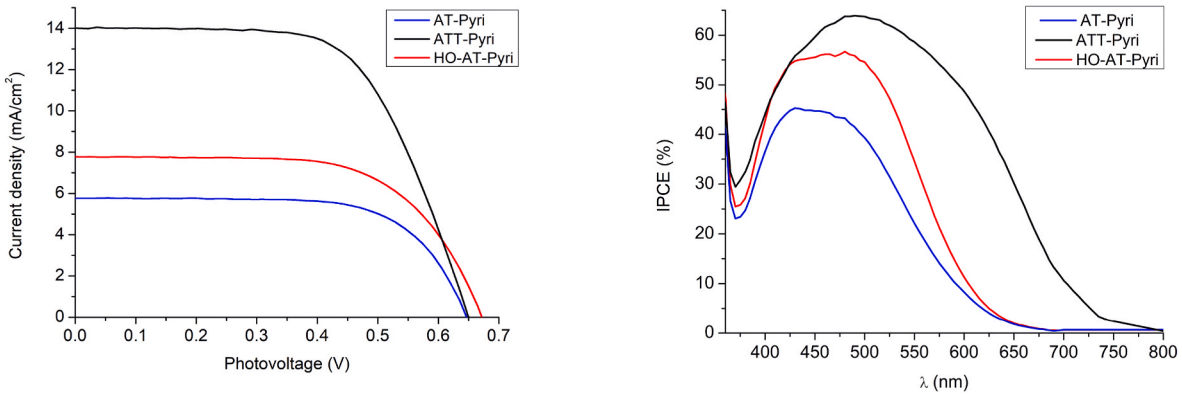

Fig. 7. Photocurrent-voltage plots (left) and IPCE (%) spectra (right) of DSSC with co-adsorbent CDCA.

Table 3
Dye loading and measured photovoltaic parameters, 24 h after assembly: open circuit voltage (V_{oc}), short circuit current density (J_{sc}), fill factor (*ff*) and overall efficiency (η). Three cells of each type were prepared and characterized (photoanode 6.5 μm).

Dye	Co-adsorbent	Dye loading (mol cm^{-2})	J_{SC} (mA cm^{-2})	V_{OC} (V)	*ff* (%)	η (%)
AT-Pyri	–	$1.26{\cdot}10^{-7}$	6.52	0.545	66.9	2.38
ATT-Pyri	–	$3.03{\cdot}10^{-7}$	9.50	0.545	63.4	3.28
HO-AT-Pyri	–	$1.53{\cdot}10^{-7}$	10.18	0.575	65.2	3.81

Table 4
Dye loading and measured photovoltaic parameters, 24 h after assembly: open circuit voltage (V_{oc}), short circuit current density (J_{sc}), fill factor (*ff*) and overall efficiency (η). Three cells of each type were prepared and characterized. (photoanode 8 μm).

Dye	Co-adsorbent	Dye loading (mol cm^{-2})	J_{SC} (mA cm^{-2})	V_{OC} (V)	*ff* (%)	η (%)
AT-Pyri	**CDCA**	$2.43{\cdot}10^{-8}$	5.76	0.650	67.1	2.51
ATT-Pyri	**CDCA**	$9.98{\cdot}10^{-8}$	14.00	0.650	62.6	5.70
HO-AT-Pyri	**CDCA**	$2.55{\cdot}10^{-8}$	7.77	0.680	62.9	3.32

1000 h after assembly. In particular, solar cells with bithiophene (**ATT-Pyri**) improve its efficiency up to 33% throughout the period of time studied.

Further studies will be carried out with this novel vinylpyrimidine as electron withdrawing anchoring group and and including bithiophene and another ancillary group such as a hydroxyl or carboxyl group due to their good electron injecting properties in these dyes for DSSCs applications.

4. Experimental section

4.1. Materials and methods

Commercial starting materials are used as received. All solvents, when necessary, are dried by standard methods.

4.1.1. *N,N-dimethyl-4-(5-(2-(pyrimidin-4-yl)vinyl)thiophen-2-yl)aniline **AT-Pyri***

A stirred mixture of aldehyde **AT-CHO** (80 mg, 0.346 mmol), 4-methylpyrimidine (32 μL, 0.346 mmol) and Aliquat 336 (16 μL, 0.035 mmol) was refluxed in 5.2 mL NaOH (5 M). After 1 h, the mixture was cooled and the precipitate was filtered off and washed with water and the aqueous phase was extracted with CH_2Cl_2 (3 × 20 mL). The organic phase was dried with $MgSO_4$ and the solvent was removed under reduced pressure. The crude product was purified by flash chromatography increasing the polarity of the eluent hexane/ethyl acetate from 8:2 to 6:4 to obtain the desired product, an orange solid (51 mg, 48%).

Molecular weight (g/mol): 307.41 **Melting point** (°C) **at 760 mm Hg**: 227.7 **IR** (KBr) ν (cm^{-1}): 1571 (C═N) **Uv–Vis data** λ_{max} (CH_2Cl_2)/nm 428 (ε/mol^{-1} dm^{3}cm^{-1} 1.98 ± 0.02·10^4) **^{1}H-NMR** ($CDCl_3$, 400 MHz) δ (ppm): 3.01 (s, 6H, NCH_3), 6.72 (d, J = 8 Hz, 2H, C_6H_4N), 6.75 (d, J = 16 Hz, 1H, CH═CH), 7.11 (d, J = 4 Hz, 1H, C_4H_2S), 7.14–7.23 (bs, 2H; C_4H_2S+$C_3H_3N_2$), 7.51 (d, J = 8 Hz, 2H, C_6H_4N), 7.99 (d, J = 16 Hz, 1H, CH═CH), 8.62 (bs, 1H, $C_3H_3N_2$), 9.11 (s, 1H, $C_3N_2H_3$) **^{13}C-NMR** ($CDCl_3$, 100 MHz) δ (ppm): 40.5 (NCH_3), 112.5 (C_6H_4N), 118.5 ($C_3N_2H_3$), 121.5 (C_4H_2S), 123.0 (CH═CH), 127.1 (C_6H_4N), 130.8 (CH═CH), 131.8 (C_4H_2S), 138.4 (4° C_4H_2S), 147.7 (4° C_4H_2S), 150.1 (4° C_6H_4N), 156.8 ($C_3N_2H_3$), 158.5 ($C_3N_2H_3$), 162.4 (4° $C_3N_2H_3$). **HRMS** (ESI)$^+$: Found [M+H]$^+$ 308.1215; molecular formula $C_{18}H_{17}N_3S$ requires [M+H]$^+$ 308.1216.

4.1.2. *N,N-dimethyl-4-(5'-(2-(pyrimidin-4-yl)vinyl)-[2,2'-bithiophen]-5-yl)aniline **ATT-Pyri***

A stirred mixture of aldehyde **ATT-CHO** (78 mg, 0.249 mmol), 4-methylpyrimidine (22 μL, 0.249 mmol) and Aliquat 336 (11 μL, 0.028 mmol) in NaOH (3.7 mL, 5 M) was refluxed for 18 h. The reaction was quenched with 30 mL H_2O and the aqueous phase was extracted with CH_2Cl_2 (3 × 20 mL). The organic phase was dried over dry $MgSO_4$. The solvent was removed by reduced pressure. The crude was purified by flash chromatography using dichloromethane: ethyl acetate 3:1. A red solid was obtained (48 mg, 49%).

Molecular weight (g/mol): 389.54 **Melting point** (°C) **at 760 mm Hg**: 264 **IR** (KBr) ν (cm^{-1}): 1578 (C═N) **Uv–Vis data** λ_{max} (CH_2Cl_2)/nm 449 (ε/mol^{-1}dm^{3}cm^{-1} 3.89 ± 0.01·10^4) **^{1}H-NMR** (400 MHz, CD_2Cl_2) δ (ppm): 2.99 (s, 6H, NCH_3), 6.73 (d, J = 8.6 Hz, 2H, C_6H_4N), 6.80 (d, J = 16 Hz, 1H, CH═CH), 7.11 (d, J = 3.6 Hz, 1H, C_4H_2S), 7.12 (d, J = 4 Hz, 1H, C_4H_2S), 7.18–7.21 (m, 2H, C_4H_2S, x2), 7.23 (d, J = 4.8 Hz, 1H, $C_4H_3N_2$), 7.48 (d, J = 8.6 Hz, 2H, C_6H_4N), 7.99 (d, J = 16 Hz, 1H, CH═CH), 8.61 (d, J = 4,8 Hz, 1H, $C_4H_3N_2$), 9.07 (s, 1H, $C_4H_3N_2$) **^{13}C-NMR** (100 MHz, CD_2Cl_2) δ (ppm): 40.7 (NCH_3), 112.9 (C_6H_4N), 119.2 ($C_4H_3N_2$), 122.1 (C_4H_2S), 122.3, 124.2 (C_4H_2S), 124.7 (CH═CH), 126.1 (C_4H_2S), 127.1, 130.3 (C_4H_2S), 131.7 (CH═CH), 134.2 (4° C_4H_2S), 139.8 (4° C_4H_2S), 140.3 (4° C_4H_2S), 151.0 (4° C_4H_2S), 152.8 (4° C_6H_4N), 157.9 ($C_4H_3N_2$), 159.4$C_4H_3N_2$), 163 (4° $C_4H_3N_2$). **HRMS** (ESI)$^+$: Found [M+H]$^+$ 390.1080; molecular formula $C_{22}H_{19}N_3S_2$ requires [M+H]$^+$ 390.1093.

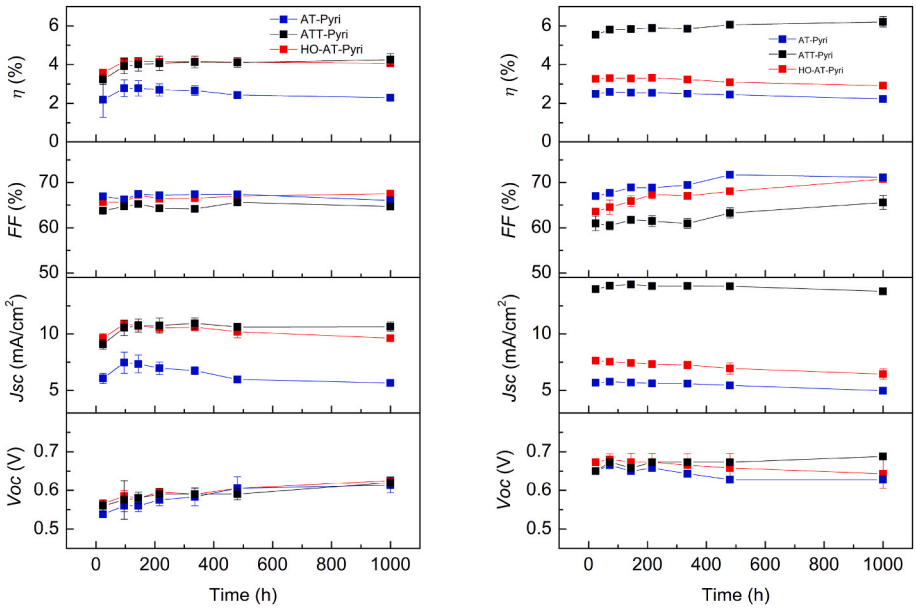

Fig. 8. Temporal evolution of the photovoltaic parameters of devices prepared with dyes **AT-Pyri, ATT-Pyri** and **HO-AT-Pyri** without (left) and with (right) CDCA with 5 h of immersion time. Measurements were performed under AM 1.5 G simulated solar light (1 sun 1000 W/m^2).

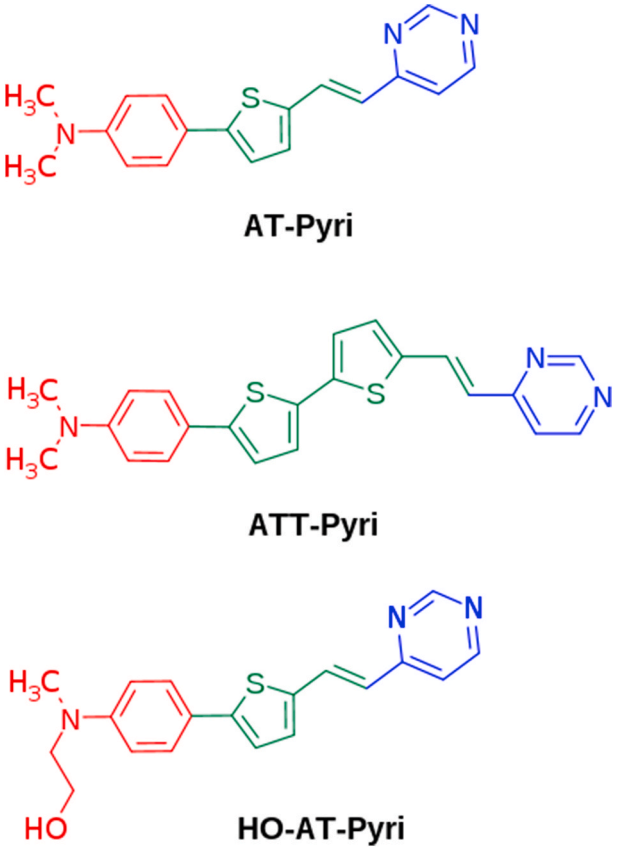

Chart 1. Chemical structures of dyes.

*4.1.3. 2-(methyl(4-(5-(2-(pyrimidin-4-yl)vinyl)thiophen-2-yl)phenyl) amino)ethanol **HO-AT-Pyri***

A stirred mixture of aldehyde **SIL-AT-CHO** (80 mg, 0.213 mmol), 4-methylpyrimidine (19.5 μL, 0.213 mmol) and Aliquat 336 (9.8 μL, 0.021 mmol) in NaOH (3.19 mL, 5 M) was refluxed for 24 h. The reaction was quenched with 30 mL H_2O and the aqueous phase was extracted with CH_2Cl_2 (3 × 30 mL). The organic phase was dried over dry $MgSO_4$. The solvent was removed by reduced pressure. The crude was purified by flash chromatography using hexane:ethyl acetate from 1:1 ratio to 3:2. A red solid was obtained (68 mg, 95%)

Molecular weight (g/mol): 337.44 **Melting point** (°C) **at 760 mm Hg**: 159–160 **IR** (KBr) ν (cm^{-1}): 3373 (O–H) **Uv–Vis data** λ_{max} (CH_2Cl_2)/nm 428 (ε/mol^{-1}dm [3] cm^{-1} 1.86 ± 0.01·10^4) **^{1}H-NMR** (CD_2Cl_2, 400 MHz) δ (ppm): 3.03 (s, 3H, NCH_3), 3.52 (d, J = 5.6 Hz, 2H, OCH_2CH_2N), 3.82 (d, J = 5.6 Hz, 2H, OCH_2CH_2N), 6.78 (d, J = 15.6 Hz, 1H, CH═CH), 6.78 (d, J = 9.0 Hz, 2H, C_6H_4N),7.14 (d, J = 3.6 Hz, 1H, C_4H_2S), 7.21 (d, J = 4 Hz, 1H, C_4H_2S), 7.22 (dd, J = 5.2 Hz, J = 1.2 Hz, 1H, $C_4H_3N_2$), 7.51 (d, J = 9 Hz, 2H, C_6H_4N), 8.01 (d, J = 15.6 Hz, 1H, CH═CH), 8.60 (d, J = 5.2 Hz, 1H, $C_4H_3N_2$), 9.06 (d, J = 1.2 Hz, 1H, $C_4H_3N_2$) **^{13}C-NMR** ($CDCl_3$, 100 MHz) δ (ppm): 39.0 (NCH_3), 55.1 (OCH_2CH_2N), 60.3 (OCH_2CH_2N), 112.8 (C_6H_4N), 118.6$C_4H_3N_2$, 121.9 (C_4H_2S), 123.1 (CH═CH) 127.2 (C_6H_4N), 130.8 (CH═CH), 131.8 (C_4H_2S), 138,4 (4° C_4H_2S), 149.9 (4° C_4H_2S), 157.3 ($C_4H_3N_2$), 158.1 (4° $C_4H_3N_2$), 158.9 ($C_4H_3N_2$), 162.3 (4° $C_4H_3N_2$). **HRMS** (ESI)$^+$: Found $[M+H]^+$ 338.1325; molecular formula $C_{19}H_{19}N_3OS$ requires $[M+H]^+$ 338.1322.

Table 5
Measured photovoltaic parameters, 1000 h after assembly: open circuit voltage (V_{oc}), short circuit current density (J_{sc}), fill factor (ff) and overall efficiency (η). Three cells of each type were prepared and characterized.

Dye	Co-adsorbent	J_{SC} (mA cm^{-2})	V_{OC} (V)	ff (%)	η (%)
AT-Pyri		5.54	0.635	65.6	2.31
AT-Pyri	**CDCA**	4.93	0.635	71.7	2.24
ATT-Pyri		11.05	0.605	65.2	4.36
ATT-Pyri	**CDCA**	13.65	0.695	67.1	6.37
HO-AT-Pyri		9.94	0.620	68.2	4.20
HO-AT-Pyri	**CDCA**	6.90	0.605	70.9	2.96

Declaration of competing interest

The authors declare that they have no known competing financial interests or personal relationships that could have appeared to influence the work reported in this paper.

Acknowledgements

We gratefully acknowledge the financial support from Gobierno de España. Ministerio de Ciencia e Innovación-MCIN/AEI/10.13039/501100011033 (Project PID2019-104307 GB-I00) and Gobierno de Aragón-Fondo Social Europeo (E47_20R). The authors are grateful to Mr L. Arnal for carring out the ATR experiments. ID and DB acknowledge for the financial support of Gobierno de Aragón-Fondo Social Europeo fellowship and PhD studentship Santander-2018 programs, respectively.

Appendix A. Supplementary data

Supplementary data to this article can be found online at https://doi.org/10.1016/j.dyepig.2022.110310.

References

[1] O'Regan B, Grätzel M. A low-cost, high-efficiency solar cell based on dye-sensitized colloidal TiO_2 films. Nature 1991;353:737–40. https://doi.org/10.1038/353737a0.
[2] Yun MJ, Cha SI, Seo SH, Lee DY. Highly flexible dye-sensitized solar cells produced by Sewing Textile electrodes on cloth. Sci Rep 2014;4:5322. https://doi.org/10.1038/srep05322.
[3] Hara K, Sato T, Katoh R, Furube A, Yoshihara T, Murai M, et al. Novel conjugated organic dyes for efficient dye-sensitized solar cells. Novel conjugated organic dyes for efficient dye-sensitized solar cells. Adv Funct Mater 2005;15:246–52. https://doi.org/10.1002/adfm.200400272.
[4] Li SL, Jiang KJ, Shao KF, Yang LM. Novel organic dyes for efficient dye-sensitized solar cells. Chem Commun 2006:2792. https://doi.org/10.1039/b603706b. 4.
[5] Liang M, Chen J. Arylamine organic dyes for dye-sensitized solar cells. Chem Soc Rev 2013;42:3453–88. https://doi.org/10.1039/C3CS35372A.
[6] Tang Y, Wang Y, Li X, Agren H, Zhu W-H, Xie Y. Porphyrins containing a triphenylamine donor and up to eight alkoxy chains for dye-sensitized solar cells: a high efficiency of 10.9. ACS Appl Mater Interfaces 2015;7:27976–85. https://doi.org/10.1021/acsami.5b10624.
[7] Duerto I, García-Palacín M, Barrios D, Garín J, Orduna J, Villacampa B. A novel σ-linkage to dianchor dyes for efficient dyes sensitized solar cells. Dyes Pigments 2020;173:107945. https://doi.org/10.1016/j.dyepig.2019.107945.
[8] Almenningen DM, Hansen HE, Buene AF, VenKatraman V, Sunde S, Hoff BH, et al. Effect of thiophene-based π-spacers on *N*-arylphenothiazine dyes for dye-sensitized solar cells. Dyes Pigments 2021;185:108951. https://doi.org/10.1016/j.dyepig.2020.108951.
[9] Li H, Fang M, Hou Y, Tang R, Yang Y, Zhong C, et al. Different effect of the additional electron-withdrawing cyano group in different conjugation bridge: the adjusted molecular energy levels and largely improved photovoltaic performance. ACS Appl Mater Interfaces 2016;8:12134–40. https://doi.org/10.1021/acsami.6b00226.
[10] Hagfeldt A, Boschloo G, Sun L, Kloo L, Pettersson H. Dye-sensitized solar cells. Chem Rev 2010;110:6595–663. https://doi.org/10.1021/cr900356p.
[11] Marotta G, Reddy MA, Singh SP, Islam A, Han L, De Angelis F, et al. Novel carbazole-phenothiazine dyads for dye-sensitized solar cells: a combined experimental and theoretical study. ACS Appl Mater Interfaces 2013;5:9635–47. https://doi.org/10.1021/am402675q.
[12] Mao J, He N, Ning Z, Zhang Q, Guo F, Chen L, et al. Stable dyes containing double acceptors without COOH as anchors for highly efficient dye-sensitized solar cells. Angew Chem Int Ed 2012;51:9873–6. https://doi.org/10.1002/anie.201204948.
[13] Ooyama Y, Inoue S, Asada R, Ito G, Kushimoto K, Komaguchi K, et al. Dye-sensitized solar cells based on a novel fluorescent dye with a pyridine ring and a pyridinium dye with the pyridinium ring forming strong interactions with nanocrystalline TiO_2 films. Eur J Org Chem 2010;1:92–100. https://doi.org/10.1002/ejoc.200900983.
[14] Zhao J, Yang X, Cheng M, Li S, Sun L. Molecular design and performance of hydroxylpyridium sensitizers for dye-sensitized solar cells. ACS Appl Mater Interfaces 2013;5:5227–31.
[15] Gou F, Jiang X, Li B, Jing H, Zhu Z. Salicylic acid as a Tridentate anchoring group for azo-bridged zinc porphyrin in dye- sensitized solar cells. ACS Appl Mater Interfaces 2013;5:12631–7.
[16] He H, Gurung A, Si L. 8-Hydroxylquinoline as a strong alternative anchoring group for porphyrin-sensitized solar cells. Chem Commun 2012;48:5910–2. https://doi.org/10.1039/C2CC31440A.
[17] Daphnomili D, Sharma GD, Biswas S, Justin TKR, Goutsolelos AG. A new porphyrin bearing a pyridinylethynyl group as sensitizer for dye sensitized solar cells. J Photochem Photobiol, A 2013;253:88–96. https://doi.org/10.1016/j.jphotochem.2012.12.013.
[18] Achelle S, Barsella A, Baudequin C, Caro B, Robin-le Guen. F. Synthesis and photophysical investigation of a series of push–pull arylvinyldiazine chromophores. J Org Chem 2012;77:4087–96. https://doi.org/10.1021/jo3004919.
[19] Wu Z, Li X, Ågren H, Hua J, Tian H. Pyrimidine-2-carboxylic acid as an electron-accepting and anchoring group for dye-sensitized solar cells. ACS Appl Mater Interfaces 2015;7:26355. https://doi.org/10.1021/acsami.5b07690. 9.
[20] Ooyama YY, Uenaka K, Ohshita J. Development of a functionally separated D–π-A fluorescent dye with a pyrazyl group as an electron-accepting group for dye-sensitized solar cells. Org Chem Front 2015;2:552–9. https://doi.org/10.1039/c5qo00050e.
[21] Chou S-H, Tsai C-H, Wu C-C, Kumar D, Wong KT. Regioisomeric effects on the electronic features of indenothiophene-bridged D–p-a'–A DSSC sensitizers. Chem Eur J 2014;20:16574–82. https://doi.org/10.1002/chem.201403584.
[22] Lin L-Y, Tsai C-H, Wong K-T, Huang T-W, Wu C-C, Chou S-H, et al. Efficient organic DSSC sensitizers bearing an electron-deficient pyrimidine as effective π-spacer. J Mater Chem 2011;21:5950. https://doi.org/10.1039/c1jm10201j. 8.
[23] Sun H, Liu D, Wang T, Li P, Bridgmohan CN, Li W, et al. Charge-separated sensitizers with enhanced intramolecular charge transfer for dye-sensitized solar cells: insight from structure-performance relationship. Org Electron 2018;61:35–45. https://doi.org/10.1016/j.orgel.2018.06.045.
[24] Costa SPG, Batista RMF, Cardoso P, Belsley M, Raposo MMM. 2-Arylthienyl-Substituted 1,3-benzothiazoles as new nonlinear optical chromophores. Eur J Org Chem 2006;17:3938. https://doi.org/10.1002/ejoc.200600059. 46.
[25] Quist F, Vande Velde CML, Didier D, Teshome A, Asselberghs I, Clays K, et al. Push–pull chromophores comprising benzothiazolium acceptor and thiophene auxiliary donor moieties: synthesis, structure, linear and quadratic non-linear optical properties. Dyes Pigments 2009;81:203–10. https://doi.org/10.1016/j.dyepig.2008.10.004.
[26] González-Laínez M, Jiménez-Ruíz MT, Martínez de Baroja N, Garín J, Orduna J, Villacampa B, et al. Using functionalized nonlinear optical chromophores to prepare NLO-active polycarbonate films. Dyes Pigments 2015;119:30–40. https://doi.org/10.1016/j.dyepig.2015.02.026.
[27] Vanden Eynde JJ, Pascal L, Van Haverbeke Y, Dubois P. Quaternary ammonium salt assisted synthesis of extended π-systems from methyldiazines and aromatic aldehydes. Synth Commun 2001;31:3167–73. https://doi.org/10.1081/SCC-100105893.
[28] Liu Z, Duan K, Guo H, Deng Y, Huang H, Yi X, et al. The enhancement of photovoltaic properties of the DSSCs based on D-A-π-A organic dyes via tuning auxiliary acceptor. Dyes Pigments 2017;140:312–9. https://doi.org/10.1016/j.dyepig.2017.01.026.
[29] Nüesch F, Grätzel M. *H*-aggregation and correlated absorption and emission of a merocyanine dye in solution, at the surface and in the solid state. A link between crystal structure and photophysical properties. Chem Phys 1995;193:1–17. https://doi.org/10.1016/0301-0104(94)00405-Y.
[30] Pazoki M, Cappel UB, Johansson EMJ, Hagfeldt A, Boschloo G. Characterization techniques for dye-sensitized solar cells. Energy Environ Sci 2017;10:672–709. https://doi.org/10.1039/c6ee02732f.
[31] Hagfeldt A, Grätzel M. Light-induced redox reactions in nanocrystalline systems. Chem Rev 1995;95:49–68. https://doi.org/10.1021/cr00033a003.
[32] Zhang L, Cole JM. Anchoring groups for dye-sensitized solar cells. ACS Appl Mater Interfaces 2015;7:3427–55. https://doi.org/10.1021/am507334m.
[33] Ooyama Y, Nagano T, Inoue S, Imae I, Komaguchi K, Ohshita J, et al. Dye-sensitized solar cells based on donor-π-acceptor fluorescent dyes with a pyridine ring as an electron-withdrawing-injecting anchoring group. Chem Eur J 2011;17:14837–43. https://doi.org/10.1002/chem.201101923.
[34] Zaki MI, Hasan MA, Al-Sagheer FA, Pasupulety L. In situ FTIR spectra of pyridine adsorbed on SiO_2-Al_2O_3, TiO_2, ZrO_2 and CeO_2: general considerations for the identification of acid sites on surfaces of finely divided metal oxides. Colloids Surf, A 2001;190:261. https://doi.org/10.1016/S0927-7757(01)00690-2.
[35] Vishwanathan V, Roh H-S, Kim J-W, Jun K-W. Surface properties and catalytic activity of TiO_2–ZrO_2 mixed oxides in dehydration of methanol to dimethyl ether. Catal Lett 2004;96:23–8. https://doi.org/10.1023/B:CATL.0000029524.94392.9f.
[36] Mohamed MM, Bayoumy WA, Khairy M, Mousa MA. Synthesis of micro–mesoporous TiO_2 materials assembled via cationic surfactants: morphology, thermal stability and surface acidity characteristics. Microporous Mesoporous Mater 2007;103:174. https://doi.org/10.1016/j.micromeso.2007.01.052.
[37] Ooyama Y, Furue K, Enoki T, Kanda M, Adachi Y, Ohshita J. Development of type-I/type-II hybrid dye sensitizer with both pyridyl group and catechol unit as anchoring group for type-I/type-II dye-sensitized solar cell. Phys Chem Chem Phys 2016;18:30662. https://doi.org/10.1039/c6cp06513a. 76.
[38] Colom E, Andrés JM, Franco S, Garín J, Montoya JF, Orduna J, et al. Multichromophoric sensitizers based on calix[4]arene scaffold and 4*H*-pyranylidene moiety for DSSCs application. Dyes Pigments 2017;136:505–14. https://doi.org/10.1016/j.dyepig.2016.08.067.
[39] Eom YK, Kanga SH, Choia IT, Kim E, Kimb J, Jua MJ, et al. New Thieno[3,2-b][1]benzothiophene-based organic sensitizers containing π-extended thiophene spacers for efficient dye-sensitized solar cells. RSC Adv 2015;5:80859–70. https://doi.org/10.1039/c5ra15100g.
[40] Buene AF, Boholm N, Hagfeldt A, Hoff BH. Effect of furan π-spacer and triethylene oxide methyl ether substituents on performance of phenothiazine sensitizers in dye-sensitized solar cells. New J Chem 2019;43:9403–10. https://doi.org/10.1039/c9nj01720h.
[41] Kern R, Sastrawan R, Ferber J, Stangl R, Luther J. Modeling and interpretation of electrical impedance spectra of dye solar cells operated under open-circuit conditions. Electrochim Acta 2002;47:4213–25. https://doi.org/10.1016/S0013-4686(02)00444-9.